INSOLATION ESTIMATES FROM GOES DATA

A REPORT

from the space science and engineering center
the university of wisconsin-madison
madison, wisconsin

INSOLATION ESTIMATES FROM GOES DATA

Final Report to Contract #NA81AA-H-00024, mod.2

Principal Investigator

Catherine Gautier

May 1983

1. Introduction

This is the final report for grant NA81AA-H-00024, mod.2 entitled : "Insolation estimates from GOES data", and it is a contribution to the AgRISTARS program of NOAA/NESS.

For practical purposes two approaches are presently available to derive insolation from geostationary satellite data: 1) a statistical method developed by Tarpley, 1979 which uses calculated correlations between mean satellite brightness measurements and ground pyranometer measurements and , 2) a physical method, developed by Gautier et al., 1980, which relies on calibrated high resolution brightness data and simple physical modeling of the radiative processes occuring in the atmosphere and clouds. The two methods have been shown to provide very similar results statistics (i.e. about 10 % of the mean surface daily insolation measurements), but the second method has the advantage that it does not require ground truth measurements. However it requires calibration of the visible sensor, good image alignment (navigation) and relatively high resolution of the brightness input data.

The main goal of this grant was to test whether a revised version of the method of Gautier et al.,1980 (later, referred as GDM for Gautier Diak and Masse) could be used with the GOES data set available at NESS, i.e. a reduced resolution hourly data set. It was initially proposed to compare the daily insolation estimates made from the GDM method applied the 48 x 48 km averaged brightness data set of NESS to a pyranometer data set to be provided by NESS. This would have however required the development of an image processing software adapted to the NESS brightness data set which we estimated would have jeopardized the complete achievement of our principal goal. Consequently, we decided to perform these tests with both the satellite and pyranometer data sets we already had used to test the GDM method. This also had the important advantage of not requiring a new calibration of the VISSR (since it had

been previously performed for the GDM study) and consequently of providing additional ressources to perform a more complete statistical analysis of the properties of insolation fields derived from satellite data.

In this report we present the results of this analysis in the context of the proposed goal of this study. In section 2 we describe the GDM method so that the reader can understand the rationale of the various tests performed. These tests and their resulting statistics (obtained by comparison with pyranometers measurements) are presented in section 3. The analysis of these results then led us in two directions: 1) the improvement of the physics of the model, which is discussed in section 4, and 2) the analysis of the natural variability of insolation, which is described in section 5. Finally, the conclusions and recommendations from this study are presented in section 6.

2. Description of the GDM method

The details of the radiative modeling are given in Gautier et al., 1980. In this section, we briefly outline the physics of the approach and in more details the procedure applied to estimate daily insolation. This will lead us to a short discussion of the sources of error in this method.

Geostationary calibrated hourly brightness data are used to derive hourly insolation in both clear and cloudy conditions. It is assumed that these data can be used to delineate cloudy regions and also to calculate the bulk radiative properties of clouds. In addition, it is assumed that in clear conditions it is possible to estimate hourly insolation from only climatological conditions, i.e. not using the measured brightness. Brightness data forming an image are thus tested, pixel by pixel, to decide whether the conditions are clear or cloudy within the radiometer field of view (pixel) using a cloud threshold value. This cloud threshold value is

obtained from the calculated surface albedo, the sun angle and the atmospheric properties. In order to reduce the amount of computation involved we assume that they are constant over a certain area and equal to the value at the center of the area. The area size (or box size) has to be large enough to noticably reduce the amount of computations, but small enough so that the variables used do not excessively vary from one side of the box to the center, i.e. such that the procedure does not introduce errors of unacceptable magnitude. For each box we determine the number of cloudy pixels (n) and their averaged cloudy brightness (B(cloudy)). The mean hourly insolation at time t for an m x m pixel box is then calculated from:

$$Ins\ (t) = (m2 - n)\ Ins(clear) + n\ Ins(cloudy)$$

where Ins(clear) is calculated using a simple model which allows one to estimate the effects of Rayleigh scattering and atmospheric water vapor absorption on solar radiation. Ins(cloudy) is calculated from B(cloudy) by applying the calibration function to obtain the corresponding cloudy reflectance R(cloudy) and the equation described in GDM. The assumption here is that Ins(cloudy) is a linear function of R(cloudy); this has been verified during the preliminary tests of the GDM method.

Thus with this approach, which represents a slight modification from that described in Gautier et al., 1980, we perform some averaging within the processing algorithm itself.

We have chosen an 8 x 8 pixel box for our typical insolation estimates because the VISSR visible sensor detector sensor is composed of an array of eight sensors. This thus allows us to use a mean calibration for all the sensors.

The daily insolation is then obtained by integrating in time the hourly insolation estimates. This integration, which is performed using the trapezoidal method, requires the determination of the sunrise and sunset times for each box of 8 x 8

pixels. These times are calculated from the satellite information contained in the directory of each image and the navigation program which relates satellite to earth coordinates.

The cloud brightness threshold, necessary to delineate cloudy regions, is calculated from the surface albedo (itself calculated from a composite clear air image in the way described in Gautier et al., 1980), to which we add an uncertainty margin in order to take into account possible changes in atmospheric conditions between the time of the analyzed picture and that of the albedo calculations. Since the brightness difference between a clear and a cloudy region is large, for any same atmospheric conditions, this approach is generally very good for delineating cloudy regions. Visual verifications have been performed which have justified our confidence in it. Fig 1 and 2 present some results from calculations made with the GDM model and compared with surface pyranometer measurements.

Error sources

The sources of error in the previously described approach are of several kinds, but in general relatively small. The most significant source of error is in representing a continuous function (insolation) by a time series of quasi-instantaneoous GOES images. Secondly, errors result from the imperfection of the radiative transfer modeling of the clouds used to calculate insolation from the brightness. These come from the fact that 1) the system is underdetermined ,i.e. we use one measurement (brightness) to infer two variables (reflectance and transmittance) and 2) the clear air modeling is relatively simplistic. Third, errors result from inaccuracy in the calibration and there is no way to verify the quality of the calibration except from intercomparison with calibrations obtained using other approaches. Fourth, errors result from the geometrical simplifications introduced in the calculation of the sun and satellite angles. Fifth, errors result from

inaccuracy in the surface albedo calculations used in the cloud threshold calculations. For large pixels errors occur because the pixel is assigned to either a clear or cloudy category, whereas it may be partially cloudy.

All these errors may add up to 20-25% on the hourly estimations.

2. Tests and resulting statistics

Since the brightness data available at NESS are spatially averaged over 8 x 8 pixels initially (and over even larger areas for the routine insolation calculations), the tests we performed with the GDM model have been made using 8 x 8 averaged brightness values as input to our model (input = 8). Various averaging combinations inside the processing algorithm (model) have then been applied . In order to have meaningfull statistics we decided to perform these tests over large enough areas and chose 64 x 64 pixels (i.e. 100 km2) area for estimating the mean insolation. This means that the insolation estimates made from the various averaging combinations inside the algorithm were all averaged in such a way that the resolution of the final mean insolation corresponds to an area of 64 x 64 pixels. The various combinations were the followings :

a)	input = 8	model = 1	final = 8
b)	= 8	= 2	= 4
c)	= 8	= 4	= 2
d)	= 8	= 8	= 1

It is important to understand the implications of all these combinations. For clarification we now explain the meaning of combination (b) for example. Since all the input data have the same resolution (i.e. average of 8 full resolution pixels), let's call this NP for New Pixel. In this case, we have used boxes of 2 x 2 NP to delineate clouds (i.e. 4 NP have been tested for clear/cloudy conditions), and the

necessary angles for our calculations have been estimated at the center of each 2 x 2 box of NP. This means that the angles have been calculated 16 times for the final 64 x 64 averaged insolation value. In the case of combination (d)only one angle has been calculated, corresponding to the center of the 64 x 64 box. The mean insolation resulting from these averaging combinations were compared to the mean insolation obtained from 1 pixel resolution input data (input = 1), averaged over 8 x 8 in the model (model = 8) and then averged over 8 x 8 (final = 8) to obtain a mean value over 64 x 64. All these results were also compared to insolation measured from a pyranometer located somewhere within that 64 x 64 box. The reason for which the pyranometer is not located in the center of the 64 x 64 box results from processing constraints (i.e. the processing always started from the top of the image). Such a processing was chosen for speed and also in order to have results in the form of images (i.e. two-dimensional arrays), from which to analyze the spatial variability. Fig 3 shows the time series of the three pyranometers used in the following comparisons. The expected error on individual insolation value is about 5 %.

Table 1 presents the daily insolation estimates for the five possible combinations tested, together with the pyranometer measurements located within the 64 x 64 pixel box for three stations in Canada over a 28 day period in may 1978. The first column indicates the mean insolation expressed in w/m2 (x24) (this unit results from a direct integration of the hourly insolation values expressed in w/m2). The second column indicates the corresponding spatial variance over the box in the same units, the third column the difference between the satellite estimate and the pyranometer measurements and the fourth column the same difference, but expressed in percentage of the pyranometer insolation.

	Ottawa				Montreal				Toronto			
Exp.	mean	var	Δ	Δ(%)	mean	var	Δ	Δ(%)	mean	var	Δ	Δ(%)
122												
1	5337	630	167	(3.0)	5019	723	-290	(6.1)	8146	217	-527	(6.9)
2	5347	632	157	(2.9)	5061	706	-332	(7.0)	8172	223	-553	(7.3)
3	5341	596	163	(3.0)	5035	597	-306	(6.5)	8150	192	-531	(7.0)
4	5327	495	177	(3.2)	4994	7	-265	(5.6)	8104	207	-485	(6.4)
5	5305	-	199	(3.6)	4989	-	-260	(5.5)	8023	-	-404	(5.3)
Pyr	5504				4729				7619			
123												
1	3144	1208	333	(9.6)	2762	715	120	(4.2)	7542	473	466	(5.8)
2	3225	1150	252	(7.2)	2811	713	71	(2.5)	7591	474	417	(5.2)
3	3193	1123	284	(8.2)	2775	597	107	(3.7)	7562	431	446	(5.6)
4	3184	979	293	(8.4)	2757	312	125	(4.3)	7513	250	495	(6.2)
5	3170	-	307	(8.8)	2761	-	121	(4.2)	7430	-	578	(7.2)
Pyr	3477				2882				8008			
124												
1	7728	335	-280	(3.8)					6755	345	-722	(12.0)
2	7771	326	-323	(4.3)					6762	346	-729	(12.1)
3	7766	288	-318	(4.3)					6744	330	-711	(11.8)
4	7761	232	-313	(4.2)					6705	223	-672	(11.1)
5	7747	-	-299	(4.0)					6654	-	-621	(10.3)
Pyr	7448								6033			
125												
1	7550	317	-914	(13.8)					1263	206	-13	(1.0)
2	7561	313	-925	(13.9)					1490	167	-240	(19.2)
3	7566	289	-930	(14.0)					1356	183	-106	(8.5)
4	7561	251	-925	(13.9)					1260	204	-10	(0.8)
5	7551	-	-915	(13.8)					1127	-	-123	(9.8)
	6636								1250			
128												
1	6151	282	-384	(7.0)					1241	231	197	(13.7)
2	6221	260	-454	(8.0)					1400	249	38	(2.6)
3	6165	249	-398	(7.0)					1288	208	150	(10.4)
4	6162	184	-395	(7.0)					1216	161	222	(15.4)
5	6081	-	-314	(5.0)					1149	-	289	(20.1)
Pyr	5767								1438			

	Ottawa				Montreal				Toronto			
Exp.	mean	var	Δ	Δ(%)	mean	var	Δ	Δ(%)	mean	var	Δ	Δ(%)
129												
1	3219	391	354	(9.9)					4741	1141	-506	(11.9)
2	3333	388	240	(6.7)					4872	1092	-637	(15.0)
3	3249	363	324	(9.1)					4807	1037	-572	(13.5)
4	3224	193	349	(9.8)					4749	790	-514	(12.1)
5	3054	-	519	(14.5)					4685	-	-450	(10.6)
Pyr	3573								4235			
130												
1	2903	347	134	(4.4)	2618	637	-575	(28.1)	4577	915	-202	(4.6)
2	3051	321	14	(0.5)	2775	581	-732	(35.8)	4645	910	-270	(6.2)
3	2932	291	105	(3.5)	2685	545	-642	(31.4)	4613	824	-238	(5.4)
4	2914	201	123	(4.1)	2673	456	-630	(30.8)	4583	750	-208	(4.8)
5	2973	-	64	(2.1)	2716	-	-673	(32.9)	4578	-	-203	(4.6)
Pyr	3037				2043				4375			
131												
1	8709	36	-708	(8.8)	8729	72	-724	(9.0)	8152	193	-981	(13.7)
2	8753	35	-752	(9.4)	8773	48	-768	(9.6)	8172	198	-1001	(14.0)
3	8749	24	-748	(9.3)	8760	55	-755	(9.4)	8150	162	-979	(13.7)
4	8740	17	-739	(9.2)	8751	32	-746	(9.3)	8088	693	-917	(12.8)
5	8735	-	-734	(9.2)	8759	-	-754	(9.4)	8017	-	-846	(11.8)
Pyr	8001				8005				7171			
133												
1	2956	470	409	(12.2)	4492	512	-86	(2.0)	2032	171	234	(10.0)
2	3112	449	253	(7.5)	4576	518	-170	(3.9)	2167	180	99	(4.5)
3	3005	418	360	(10.7)	4508	416	-102	(2.3)	2080	152	186	(8.2)
4	2892	419	473	(14.1)	4503	35	-97	(2.2)	2012	78	254	(11.2)
5	2711	-	654	(19.4)	4473	-	-67	(1.5)	1940	-	326	(14.4)
Pyr	3365				4406				2266			
135												
1	2254	347	607	(21.2)	2246	774	876	(28.1)	3568	1677	-1242	(53.4)
2	2407	298	454	(15.9)	2478	748	644	(20.6)	3668	1593	-1342	(57.7)
3	2319	304	542	(18.9)	2344	713	778	(24.9)	3627	1584	-1301	(55.9)
4	2263	277	598	(20.9)	2238	653	884	(28.3)	3562	1401	-1236	(53.1)
5	2294	-	567	(19.8)	2117	-	1005	(32.2)	3615	-	-1289	(55.4)
Pyr	2861				3122				2326			

	Ottawa				Montreal				Toronto			
Exp.	mean	var	Δ	Δ(%)	mean	var	Δ	Δ(%)	mean	var	Δ	Δ(%)
136												
1	7884	575	-180	(2.3)	5747	870	-1119	(16.3)	4556	636	-1420	(45.3)
2	7947	573	-243	(3.2)	5832	871	-1034	(15.1)	4646	617	-1510	(48.2)
3	7938	554	-234	(3.0)	6250	385	-616	(9.0)	4598	576	-1462	(46.6)
4	7923	438	-219	(2.8)	6228	146	-638	(9.3)	4522	457	-1386	(44.2)
5	7910	-	-206	(2.7)	6223	-	-643	(9.4)	4532	-	-1396	(44.5)
Pyr	7704				6866				3136			
138												
1	5185	559	-654	(14.4)	4566	873	128	(2.7)	4423	669	-55	(1.3)
2	5277	530	-746	(16.5)	4692	837	2	(-)	4510	737	-142	(3.3)
3	5223	490	-692	(15.3)	4617	780	77	(0.1)	4473	669	-105	(2.4)
4	5192	412	-661	(14.6)	4604	486	90	(1.9)	4440	519	-72	(1.6)
5	5142	-	-611	(13.5)	4581	-	113	(2.5)	4428	-	-60	(1.4)
Pyr	4531				4694				4368			
141												
1	8794	219	-784	(9.8)	7246	582	-216	(3.1)	8753	300	-387	(4.6)
2	8847	219	-837	(10.4)	7299	587	-269	(3.8)	8786	283	-420	(5.0)
3	8846	204	-836	(10.4)	7277	539	-247	(3.5)	8765	272	-399	(4.6)
4	8839	177	-829	(10.3)	7264	516	-234	(3.3)	8713	145	-347	(4.1)
5	8830	-	-820	(10.2)	7250	-	-220	(3.1)	8610	-	-244	(2.9)
Pyr	8010				7030				8366			
139												
1	8707	315	-791	(10.0)	8934	115	-1475	(19.8)	8892	178	-977	(12.3)
2	8768	323	-852	(10.8)	8998	122	-1539	(20.6)	8938	181	-1023	(12.9)
3	8767	305	-851	(10.8)	8995	105	-1536	(20.6)	8917	143	-1002	(12.7)
4	8756	239	-840	(10.6)	8976	63	-1517	(20.3)	8845	137	-930	(11.7)
5	8747	-	-831	(10.5)	8991	-	-1532	(20.5)	8735	-	-820	(10.4)
Pyr	7916				7459				7915			
140												
1	6574	344	-1330	(25.4)	6731	354	-978	(17.0)	3605	844	-802	(28.6)
2	6589	346	-1345	(25.6)	6768	370	-1015	(17.6)	3669	829	-866	(30.9)
3	6573	310	-1329	(25.3)	6747	302	-994	(17.3)	3611	830	-808	(28.8)
4	6542	251	-1298	(24.8)	6722	194	-969	(16.8)	3580	771	-777	(27.7)
5	6526	-	-1282	(24.4)	6731	-	-978	(17.0)	3542	-	-739	(26.4)
Pyr	5244				5753				2803			

	Ottawa				Montreal				Toronto			
Exp.	mean	var	Δ	Δ(%)	mean	var	Δ	Δ(%)	mean	var	Δ	Δ(%)
137												
1	1815	405	-485	(36.5)	4587	1115	-94	(2.1)	4901	1209	-960	(24.4)
2	2024	375	-694	(52.2)	4724	1072	-231	(5.1)	5029	1159	-1088	(27.6)
3	1825	407	-495	(37.2)	4633	1027	-140	(3.1)	4950	1074	-1009	(25.6)
4	1697	323	-367	(27.6)	4632	823	-139	(3.1)	4920	384	-979	(24.8)
5	1536	-	-206	(15.5)	4504	-	-11	(0.2)	4916	-	-975	(24.7)
Pyr		1330			4493				3941			
142												
1	9040	64	-723	(8.7)	8975	97	-494	(5.8)	9047	105	-813	(9.9)
2	9094	63	-777	(9.3)	9041	97	-560	(6.6)	9094	93	-860	(10.4)
3	9087	40	-770	(9.3)	9028	60	-547	(6.4)	9062	105	-828	(10.1)
4	9080	10	-763	(9.2)	9010	38	-529	(6.2)	9000	91	-766	(9.3)
5	9072	-	-755	(9.1)	9021	-	-540	(6.4)	8873	-	-639	(7.8)
Pyr	8317				8481				8234			
143												
1	9025	78	-1171	(14.9)	8775	154	-794	(9.9)	7951	368	-543	(7.3)
2	9071	73	-1217	(15.5)	8822	147	-841	(10.5)	7965	370	-557	(7.5)
3	9068	53	-1214	(15.5)	8814	117	-833	(10.4)	7946	330	-538	(7.3)
4	9066	28	-1212	(15.4)	8802	42	-821	(10.3)	7899	271	-491	(6.6)
5	9061	-	-1207	(15.4)	8812	-	-831	(10.4)	7841	-	-433	(5.8)
Pyr	7854				7981				7408			
144												
1	9086	53	-1194	(15.1)	9123	78	-1206	(15.2)	8484	251	-1034	(13.9)
2	9109	53	-1217	(15.4)	9159	64	-1242	(15.7)	8492	252	-1042	(14.0)
3	9111	29	-1219	(15.4)	9147	62	-1230	(15.5)	8470	225	-1020	(13.7)
4	9107	20	-1215	(15.4)	9133	14	-1216	(15.4)	8418	207	-968	(13.0)
5	9097	-	-1205	(15.3)	9146	-	-1229	(15.5)	8338	-	-888	(11.9)
Pyr	7892				7917				7450			
145												
1	9078	90	-1267	(16.2)	9130	88	-1209	(15.3)	9201	68	-858	(10.3)
2	9130	98	-1319	(16.9)	9192	83	-1271	(16.0)	9239	53	-896	(10.7)
3	9125	76	-1314	(16.8)	9184	69	-1263	(15.9)	9209	70	-866	(10.4)
4	9117	60	-1306	(16.7)	9154	40	-1233	(15.6)	9140	105	-797	(9.6)
5	9105	-	-1294	(16.6)	9174	-	-1253	(15.8)	9011	-	-668	(8.0)
Pyr	7811				7921				8343			

	Ottawa				Montreal				Toronto			
Comb.	mean	var	Δ	Δ(%)	mean	var	Δ	Δ(%)	mean	var	Δ	Δ(%)
146												
1-8-8	8210	226	-1058	(14.8)	8217	225	-1364	(19.9)	8936	143	-832	(10.3)
8-1-8	8232	221	-1080	(15.1)	8237	234	-1384	(20.2)	8961	149	-857	(10.6)
8-2-4	8232	178	-1080	(15.1)	8234	203	-1381	(20.2)	8935	114	-831	(10.3)
8-4-2	8226	134	-1074	(15.0)	8222	77	-1369	(20.0)	8873	93	-769	(9.6)
8-8-1	8218	-	-1066	(14.9)	8227	-	-1374	(20.0)	8783	-	-679	(8.4)
	7152				6853				8104			
148												
1-8-8	8171	92	-477	(6.2)	8079	111	-287	(3.7)	8467	67	-188	(2.3)
8-1-8	8201	108	-507	(6.6)	8131	128	-339	(4.4)	8505	57	-226	(2.7)
8-2-4	8201	90	-507	(6.6)	8118	89	-326	(4.2)	8473	67	-194	(2.3)
8-4-2	8197	74	-503	(6.5)	8090	34	-298	(3.8)	8417	102	-138	(1.7)
8-8-1	8188	-	-494	(6.4)	8098	-	-306	(3.9)	8285	-	-6	(0.1)
Pyr	7694				7792				8279			
149												
1-8-8	8214	337	-948	(13.0)	7627	1344	226	(2.9)	8131	95	-328	(4.2)
8-1-8	8270	347	-1004	(13.8)	7706	1321	147	(1.9)	8168	101	-365	(4.7)
8-2-4	8380	319	-1114	(15.3)	7812	1354	41	(0.5)	8143	78	-340	(4.4)
8-9-2	8376	310	-1110	(15.3)	7762	1232	91	(1.2)	8091	95	-288	(3.7)
8-8-1	8827	-	-1561	(21.5)	8269	-	-416	(5.3)	7998	-	-195	(2.5)
Pyr	7266				7853				7803			
150												
1-8-8	8530	261	-1337	(18.6)	8650	307	-2292	(36.0)	8535	289	-746	(9.6)
8-1-8	8538	245	-1345	(18.7)	8709	285	-2351	(37.0)	8552	308	-763	(9.8)
8-2-4	8540	176	-1347	(18.7)	8700	183	-2342	(36.8)	8534	280	-745	(9.6)
8-4-2	8537	113	-1344	(18.7)	8675	46	-2317	(36.4)	8478	192	-689	(8.8)
8-8-1	8528	-	-1335	(18.6)	8684	-	-2326	(36.6)	8436	-	-647	(8.3)
Pyr	7193				6358				7789			

The statistics of the entire data set are presented in Table 2. From table 1, 2 and fig 4 (which represent the distribution of the difference between the satellite estimates and the pyranometer measurements for three of the 5 tested combinations), it is clear that this difference is relatively small (r.m.s of 9 to 10% of the mean pyranometer measurements). It was not expected however to find the close agreement obtained between the results from the full resolution calculations and the

results obtained using mean input 8 x 8 brightness. This seems to indicate a quasi-linearity between brightness and insolation for that space scale (about 100 km at this latitude) and this could explain the quality of the results obtained from a statistical model which uses mean brightness and takes into account the geometry of the problem (i.e. Tarpley's approach).

Table 2.

	$\underline{A}$(%)	$\sqrt{\sigma}$ ($\underline{A}$)	$\sqrt{\sigma}$ ($\underline{I}$)
1-8-8	12.2	9	416
8-1-8	12.5	9	403
8-2-4	12.2	9	-
8-4-2	12.0	-	275
8-8-1	12.2	-	-
closest	11.8	10	-
mean insolation from pyranometer = 5922 $\underline{WD}/m^2$			

This quasi-linearity may result from the fact that, in the cases tested, the values of brightnesses encountered were within a limited range (e.g. relatively homogeneous cloud cover or combinations of relatively high surface albedos and small clouds). We have however eliminated this possibility by examining low surface albedo regions such as the Lake Ontario region in our image. Table 3 shows the summary of the results obtained in the lake area for only 2 combinations (i.e. 1-8-8 and 8-1-8). Clearly the insolation estimates for these two combinations are very similar.

Table 3.

Lake Ontario

	122			123			124			125		
1-8-8	7775		400	6583		263	7320		183	2128		390
8-1-8	7661		-	6506		-	7218		-	2193		-
	128			129			130			131		
1-8-8	3392		507	3359		494	5778		1008	8754		64
8-1-8	3232		-	3047		-	5708		-	8634		-
	133			135			136			137		
1-8-8	3836		893	3270		940	3386		336	3161		364
8-1-8	3866		-	3197		-	3331		-	2954		-
	138			141			140			142		
1-8-8	4351		1397	8452		412	6022		411	9123		49
8-1-8	4316		-	8348		-	5942		-	9006		-
	143			144			145			146		
1-8-8	8783		191	7868		272	9112		80	8509		100
8-1-8	8669		-	7754		-	8985		-	8375		-
	148			149			150			151		
1-8-8	8339		95	8166		97	8973		134	6902		256
8-1-8	8229		-	8057		-	8863		-	6808		-
	129			147			132					
1-8-8	3456		593	8500		114	1613		188			
8-1-8	3231		-	8383		-	1355		-			

The close correspondence between the results of the two methods (averaged data/averaged insolation) when compared with pyranometers measurements could also be due to the fact that mean insolations over a 64 x 64 box estimated from the two methods are closer to each other than they are to measurements of insolation by a pyranometer at a single location. This explanation can be tested by comparing the pyranometer measurements to the estimates made using full resolution input brightness for the box located the closest to the pyranometer location. Such comparisons are presented in table 4.

Table 4.

	Ottawa	Montreal	Toronto	Ottawa	Montreal	Toronto
Day		122			123	
pyr	5504	4729	7619	3477	2882	8008
closest	5266	4845	7977	2175	2970	7600
Δ(%)	4	2	5	37	3	5
Δ (WD/m^2)	238	-116	-358	1302	-88	408
Day		124			125	
pyr	7448	-	6033	6636	-	1250
closest	7646	-	6749	7336	-	1217
Δ(%)	3	-	12	11	-	3
Δ	-198	-	-716	-700	-	33
Day		128			129	
pyr	5767	-	1438	3573	-	4235
closest	5967	-	1196	3066	-	3726
Δ(%)	3	-	17	14	-	12
Δ	-200	-	242	507	-	509
Day		130			131	
pyr	3037	2043	4375	8001	8005	7171
closest	2691	2124	4209	8675	8758	7782
Δ(%)	11	4	4	8	9	9
Δ	346	-81	166	-674	-753	-611
Day		133			135	
pyr	3365	4406	2266	2861	3122	2326
closest	2586	5399	2028	2828	2987	2344
Δ(%)	23	23	11	1	4	1
Δ	779	-993	238	33	135	-18
Day		136			137	
pyr	7704	6866	3136	1330	4493	3941
closest	8234	4330	3720	1662	3595	5371
Δ(%)	7	37	19	25	20	36
Δ	-530	2536	-584	-332	898	-1430
Day		138			141	
pyr	4531	4694	4368	8010	7030	8366
closest	4617	4384	4477	9054	7830	8763
Δ(%)	2	7	2	13	11	5
Δ	-86	310	-109	-1044	-800	-397

	Ottawa	Montreal	Toronto	Ottawa	Montreal	Toronto
Day		139			140	
pyr	7916	7459	7915	5244	5753	2803
closest	9032	9022	9028	6316	6123	2346
Δ(%)	14	21	14	20	6	16
Δ	-1116	-1563	-1113	-1072	-370	457
Day		142			143	
pyr	8317	8481	8234	7854	7981	7408
closest	8927	9008	9173	9026	8850	8026
Δ(%)	7	6	11	15	11	8
Δ	-610	-527	-939	-1172	-869	-618
Day		144			145	
pyr	7892	7917	7450	7811	7921	8343
closest	9025	9209	8725	9101	9279	9280
Δ(%)	14	16	17	17	17	11
Δ	-1133	-1292	-1275	-1290	-1358	-937
Day		146			148	
pyr	7152	6853	8104	7694	7792	8279
closest	8226	8258	9000	8140	8254	8499
Δ(%)	15	21	11	6	6	3
Δ	-7642-1074	-1405	-896	-446	-462	-220
Day		149			150	
pyr	7266	7853	7803	7193	6358	7789
closest	8212	9270	8235	8551	8622	8855
Δ(%)	13	18	6	19	36	14
Δ	-946	-1417	-432	-1358	-2264	-1066
Day		151			147	
pyr	4236	5624	7253	7674	8090	8099
closest	4121	6521	7704	8471	8624	8574
Δ(%)	3	16	6	10	7	6
Δ	115	-897	-451	-797	-534	-475
Day		132				
pyr	2017	4406	1551			
closest	2158	4829	1299			
Δ(%)	7	10	16			
Δ	-141	-423	252			

The first column indicates the pyranometer measurement, the second is the "closest", the third gives the difference between the "closest" and the pyranometer and the fourth column the same difference, expressed in percentage of the pyranometers meas-

urements. Again, the results were not anticipated since the r.m.s of the difference is even larger than that for the spatial averages over 64 x 64. In order to understand these results we need to look in more details at each individual case in order to infer the reasons for this situation.

We carefully examined the cases for which the difference (in percent) of the previous comparisons ("closest" vs pyranometers) w ere larger than 15%. We found two classes of errors. First, a class for which the spatial variability was very large (as deduced from the estimated spatial variance). In these cases it was always possible to find an adjacent box for which the satellite insolation estimate was within a few percent of the pyranometer measurements. Second, a class for which the discrepancy between the satellite estimates and the pyranometers measurements occur when the insolation is large; most of the time larger than 7500 w/m2 (x24). In these cases the spatial variability was relatively small and the conditions were almost clear, although not entirely. Examination of the cloud albedos obtained in the intermediary calculations of the model showed that they were in the vicinity of 3 to 6 %. We interpreted this as corresponding to partial filling of the 1 km pixel. Visual examination of the images corresponding to these cases enhanced our confidence in this explanation.

From these two kinds of results it became evident to us that two further steps were necessary to better interpret these results :

1) to improve our modeling in the quasi-clear air conditions and,

2) to study the effects of data averaging on the spatial characteristics of insolation, since we have seen that we could retrieve the mean value relatively precisely with an averaged input brightness.

The results obtained from these two steps are presented in the following two sections (section 4 and 5).

4. Improved insolation model

4a. Model improvements

Since we needed to modify our modeling in quasi-clear air conditions, we also added improvements which related to the important simplifications of the original model, i.e. :

1) No separation of broad-band solar fluxes and intensities specific to the GOES sensor(VISSR) band width. Broad-band solar parameterization used for water vapor absorption and Rayleigh scattering.

2) Isotropic scattering and reflection.

3) No clear-air absorption process besides water vapor absorption.

4) Plane parallel clouds which fill the sensor field-of-view.

In calculating quantities derived from the VISSR brightness measurement (surface albedo,cloud threshold and cloud albedo) simple parameterizations of the physical processes within the VISSR bandwidth replace the previous broad-band assumptions.

In this spectral region, water vapor has only a weak absorption band at .7 microns and the sensor sensitivity is low at this wavelength. Thus, water vapor absorption is neglected in calculating the surface albedo, threshold and cloud albedo. The broad-band absorption of solar flux (Paltridge, 1973) is retained in the calculation of surface insolation.

Ozone absorption (bands in the ultraviolet and visible) was neglected in the original model. While the effect of ozone absorption on the total solar flux is small (2%), the effect of the visible ozone absorption band on the flux in the VISSR channel may be more important. Ozone absorption was modelled in the manner of Lacis and Hansen (1974), considering the ozone layer as an absorbing medium overlying a reflection layer (the earth-atmosphere system). The empirical formula in Lacis and Hansen (1974) for ozone absorption in the visible region is used to estimate the absorption in the VISSR channel for the calculation of surface albedo, threshold and cloud albedo. This formula plus a counterpart for ozone absorption in the ultraviolet together describe the effects of ozone on the total solar flux for calculation of insolation.

To estimate the effect of Rayleigh scattering of the direct solar beam in the VISSR channel, a single-scattering approximation to the Rayleigh scattered intensity at the VISSR peak sensitivity wavelength (.6 microns) is used (Coulson 1959). Its magnitude is a function of the Rayleigh scattering optical depth of the atmosphere at that wavelength and the satellite, sun and relative angles. Backscattering of diffuse flux in the VISSR channel is estimated at this optical depth from the tables of Coulson(1959).

In the case of cloud, all scattering processes are assigned above cloud top which we fix at about 700 mb. The magnitude of the scattering is adjusted by lowering the Rayleigh scattering optical depth to represent the fraction of atmospheric mass above cloud tops. In the equation for surface insolation, the original broadband solar estimates of Rayleigh scattering are retained.

In addition to the improved physics, a simple correction for clouds smaller than the sensor field-of-view has been added. A systematic overestimation of insolation (i.e. underestimation of cloud albedo) was found in the results presented and

discussed earlier. This is understandable since the insolation model is designed for plane-parallel clouds which are assumed to fill the sensor field of view. The leakage of energy out the sides of finite clouds is a well-known phenomenon. Much of this energy out the sides, while directed to the upward hemisphere is in directions away from the satellite angle and is therefore not accounted for in the model calculation of cloud albedo from measured brightness. An erroneously low cloud albedo value and overestimate of insolation is the result.

To correct this condition, we have imposed a minimum cloud albedo of 7% when any clouds at all are detected (i.e. data brightness above calculated cloud threshold).

A maximum cloud absorption of 7% of the incident flux at cloud top for the brightest(thickest) clouds produced better results in the new model than did the old model maximum of 20%. With the improved model physics we found that the statistical correction for thick and extensive clouds required in the old model was no longer necessary.

4b. Results

The results of model improvements on the calculation of insolation were evaluated by reprocessing seven days of the original Canadian data set (three pyranometer locations per day) with the new model. The days encompass conditions ranging from very clear to very cloudy.

In processing the Canadian data set originally with the old model, days with marginal navigation quality were left in so as to have an indication of the total errors associated with the satellite methods. In selecting days to reprocess with the new model, those for which the navigation was at all suspect were purposely eliminated so that the merits of the different physical models could be compared,

minimizing error effects of navigation problems.

The results of these improvements of the model are presented in table 5.

Table 5.

Ottawa					
day	pyr	"closest"	Δ(%)	new	Δ(%)
135	2861	2828	(1)	2777	(3)
138	4531	4617	(2)	4495	(1)
139	7416	9032	(14)	8044	(2)
140	5244	6316	(20)	5994	(14)
144	7892	9025	(14)	8132	(3)
146	7152	8226	(15)	7531	(5)
Montreal					
day	pyr	"closest"	Δ(%)	new	Δ(%)
135	3122	2987	(4)	3002	(4)
138	4694	4384	(7)	4463	(5)
139	7459	9022	(21)	7937	(6)
140	5753	6123	(6)	5723	(.5)
144	7917	9209	(16)	8132	(3)
146	6853	8258	(21)	7541	(10)
Toronto					
day	pyr	"closest"	Δ(%)	new	Δ(%)
135	2326	2344	(1)	2364	(2)
138	4368	4477	(2)	4480	(3)
139	7915	9028	(14)	8040	(2)
140	2803	2345	(16)	2230	(20)
144	7450	8725	(17)	7961	(7)
146	8104	9000	(11)	8065	(5)

For daily insolation the new model outperformed the best version of the old model in 16 of 21 trials (not all presented in the table). The standard error of measurement in satellite estimated daily insolation vs. pyranometers was 5.3% for the new model. For the same days the best version of the old model (systematic error removed)

yielded a standard error of 6.3%. The removal of systematic error from the new model has yet to be performed and this should lead to some additional improvement. Once the new physical parameterizations are put in look-up tables form, we anticipate no increase in computer time for this improved model.

5. Spatial variability

Since the average of insolation seems to be relatively well estimated by the various combinations discussed earlier, it is important to verify that the important spatial characteristics of insolation are also conserved in the various schemes. This was studied from an analysis of the estimated spatial variance, presented in Table 1, and from a structure function analysis of the fields obtained using the various combinations.

5.a Analysis of the variance

Examination of Table 1 indicates that in cases of cloudy conditions the spatial variance can be quite large. A previous study of that variance (Gautier, 1982) has showed that is was about 30 % of the mean insolation value. The use of 8 pixels averages as input data reduces the variance by a few % for the 8-1-8 combination and by 10-20 % for the 8-4-2 combination, which is the combination that contains the largest spatial averaging, for which we can calculate the variance (in the case 8-8-1, insolation is calculated by averaging 8 boxes inside the model, therefore no spatial variance can be estimated). From this analysis, we can conclude that the spatial variance is not well conserved by the various processing combination, with a possible loss of spatial variability information of up to 40 %. A structure analysis will thus indicate the characteristics of this loss of spatial spatial information.

5b. Structure function analysis

Structure functions D(d) are defined as :

$$D_{II}(d) = \overline{(I(r+d) - I(r))^2}$$

where the overbar denotes an averaging operator. They express the spatial variations as a function of distance d in all possible directions (360).

We calculated the two-dimensional structure functions of insolation for fields corresponding to each combination and, for simplification of the interpretation the one-dimensional mean structure function for the zonal and meridional directions.

The fields of insolation for the various combinations are presented in fig 5, 6, 7, 8 and 9 for respectively 1-8,8-1,8-2,8-4 and 8-8 As expected there is a decrease of the spatial details from the first to the last combination. The corresponding two-dimensional structure functions are presented in fig 10,11,12,13 and 14. The spatial details showed in fig 10 are well reproduced for the combinations up to 8-4, but in 8-8 there is some aliasing introduced by the poor spatial sampling. For instance the feature that extends in the south-east north-west direction at small scales (10 to 40 in the units of the graph) is distorted and the scales are not well represented. At larger scales, the feature in the north-eat corner is very distorted. This analysis suggests that an average of 8 within the model is too large for the insolation field we have analyzed here.

The one-dimensional structure function analysis is presented on fig 15 and 16. These results indicate that in the meridional direction there is some distortion at the small scale but very little at the large scales (beyond 100 km). On the other hand, in the zonal direction the distortion is important at all scales and, as for the two-dimensional analysis, the 8-8 combination has an important degradation of the information even at large scales.

6. Conclusions and recommendations

The results presented and discussed above indicate that spatially averaged daily insolation can be estimated from mean hourly brightness at a resolution of about 14 km (averages of eight full resolution pixels). These results have been obtained by spatially averaging original full resolution (about 1.7 km) brightness data, but the same conclusions would probably hold for sensor-averaged brightness provided that the sensor averaging procedure is sufficiently isotropic.

Since our results seem to indicate a quasi-linearity between linear combinations of hourly brightness and daily insolation at the 100 km scale and since the results of combination 8-1-8 are comparable to the other resultsfor the mean insolation, it appears that it may be even possible to use input hourly brightness averaged over as large an area as 100 km to obtain adequate mean insolation values. However, the spatial analysis indicates that, for the particular insolation fields analyzed here, the 8-8 combination distorts the field extensively but not the 8-4.

Therefore we conclude that the optimal averagings of the input data and within the model which require the least amount of computation but retain the important spatial characteristics of the field analyzed are an average of eight (8) of the input hourly brightness with an average of four (4) within the model to calculate hourly and daily insolation.

Obviously, these results still require further testing with larger data sets to ensure their statistical representativity, and their validity for other insolation fields. the spatial field analysis, as a function of its spatial characteristics.

REFERENCES

Coulson, K.L., 1959. Characteristics of the radiation emerging from the top of a Rayleigh atmosphere, 1 and 2. Planet. Space Sci., 1, 256-284.

Gautier, C., 1982. Mesoscale Insolation Variability Derived from Satellite Data. Jour. Appl. Meteor. 21, 51-58.

Gautier, G., G. Diak and S. Masse, 1980. A Simple Physical Model to Estimate Incident Solar Radiation at the Surface from GOES Satellite Data. Jour. Appl. Meteor., 19, 1005-1012.

Lacis, A.A. and J.E. Hansen, 1974. A parameterization for the absorption of solar radiation in the earth's atmosphere. J. Atmos. Sci., 31, 118-133.

Paltridge, G.W., 1973. Direct measurement of water vapor absorption of solar radiation in the free atmosphere. J. Atmos. Sci., 30, 156-160.

Tarpley, J.D., 1979: Estimating incident solar radiation at the surface from geostationary satellite data. J. Appl. Meteor., 18, 1172-1181.

Figures

Fig 1 : Insolation variation with time for day 110 1978

Broken lines = satellite estimates,

Stepwise lines = pyranometers measurements

Fig 2 : Insolation variation with time for day 240 1978

Broken lines = satellite estimates,

Stepwise lines = pyranometers measurements

Fig 3 : Pyranometers Daily INsolation Time Series

for Ottawa, Montreal and Toronto during the time period of the experiments.

Fig 4 : Distribution of the Normalized Difference:

(Pyrano. meas. - Satellite est.)/Pyrano. meas. for various experiments

Fig 5 : Insolation Field for Day 123 1978

Experiment number 1

Fig 6 : Insolation Field for Day 123 1978

Experiment number 2

Fig 7 : Insolation Field for Day 123 1978

Experiment number 3

Fig 8 : Insolation Field for Day 123 1978

Experiment number 4

Fig 9 : Insolation Field for Day 123 1978

Experiment number 5

Fig 10 : 2-Dim Structure Function of Insolation Field

for Day 123 1978 Experiment number 1

Fig 11 : 2-Dim Structure Function of Insolation Field

for Day 123 1978 Experiment number 2

Fig 12 : 2-Dim Structure Function of Insolation Field

for Day 123 1978

Experiment number 3

Fig 13 : 2-Dim Structure Function of Insolation Field for Day 123 1978

Experiment number 4

Fig 14 : 2-Dim Structure Function of Insolation Field for Day 123 1978

Experiment number 5

Fig 15 : Meridional Structure Function for Day 123 1978

Fig 16 : Zonal Structure Function for Day 123 1978

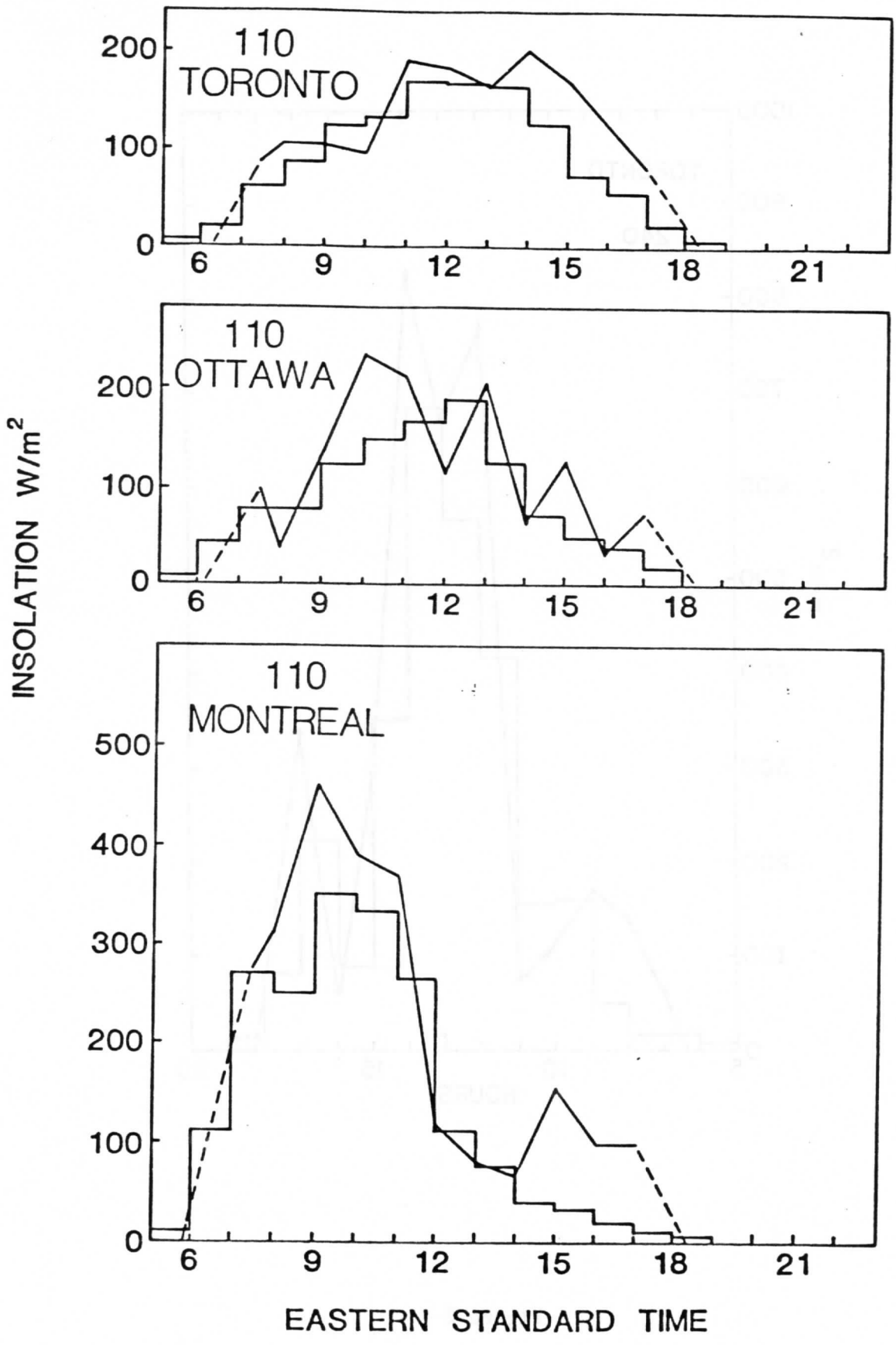
110
TORONTO
200
100
0
6
9
12
15
18
21
110
OTTAWA
200
100
0
6
9
12
15
18
21
110
MONTREAL
500
400
300
200
100
0
6
9
12
15
18
21
INSOLATION W/m²
EASTERN STANDARD TIME

Figure 1

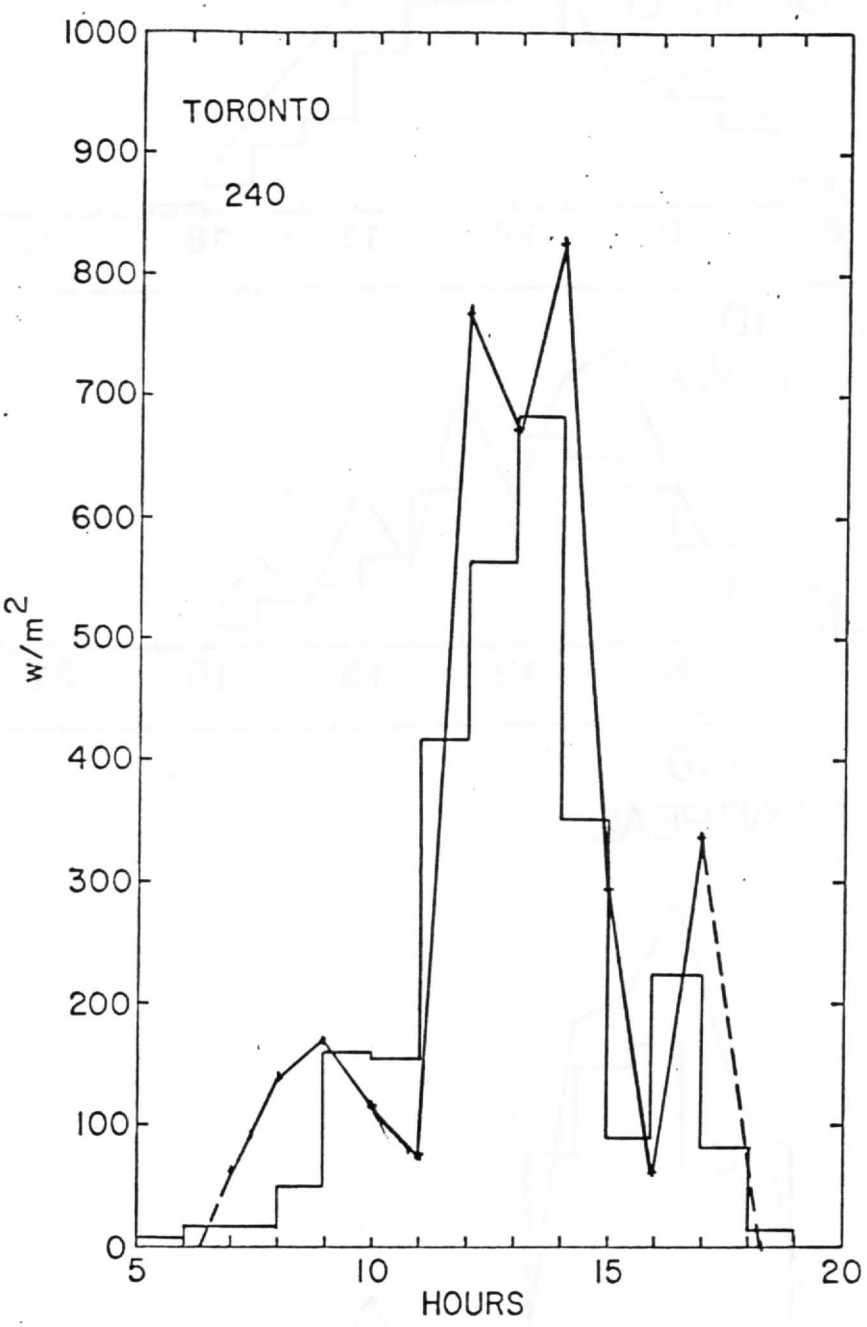
TORONTO
240
1000
900
800
700
600
500
400
300
200
100
0
w/m2
5
10
15
20
HOURS

Figure 2

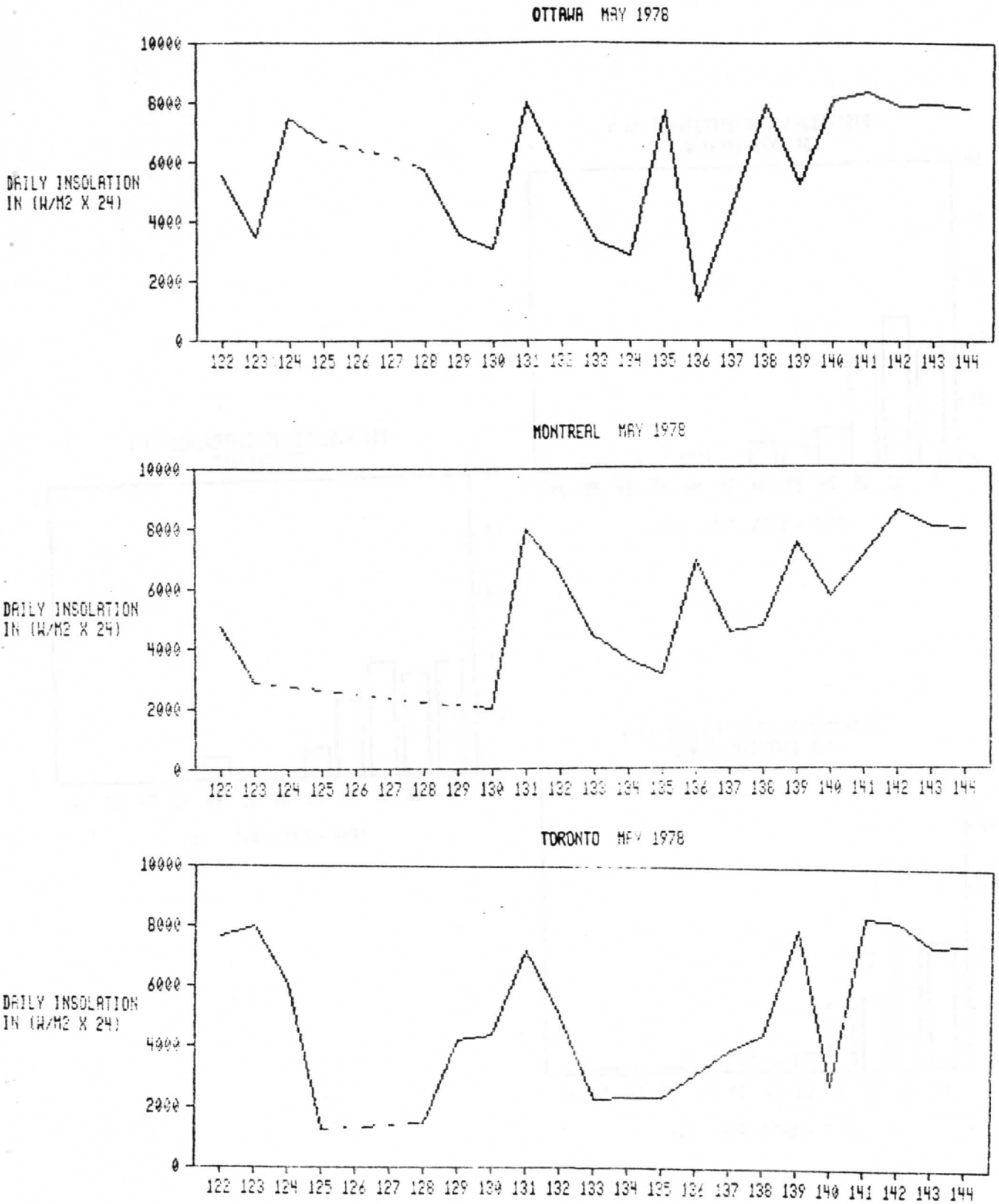
OTTAWA MAY 1978
MONTREAL MAY 1978
TORONTO MAY 1978
DAILY INSOLATION IN (W/M2 X 24)
10000
8000
6000
4000
2000
0
122 123 124 125 126 127 128 129 130 131 132 133 134 135 136 137 138 139 140 141 142 143 144
JULIAN DAYS

Figure 3

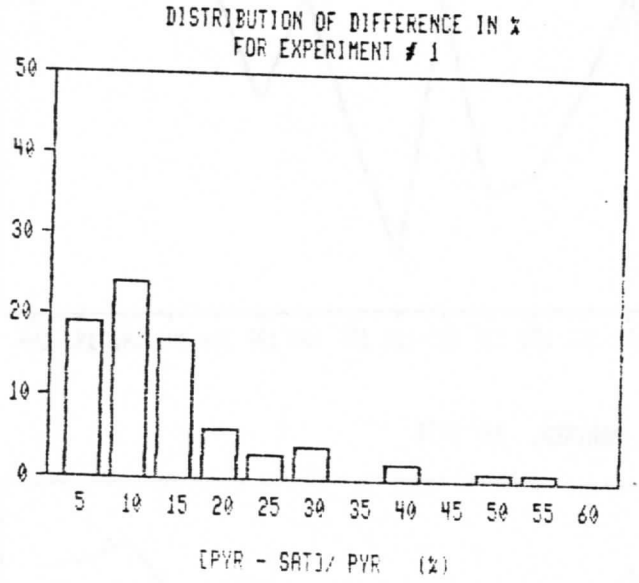
DISTRIBUTION OF DIFFERENCE IN %
FOR EXPERIMENT # 1
NUMBERS
NUMBERS
50
40
30
20
10
0
5 10 15 20 25 30 35 40 45 50 55 60
[PYR - SAT]/ PYR (%)

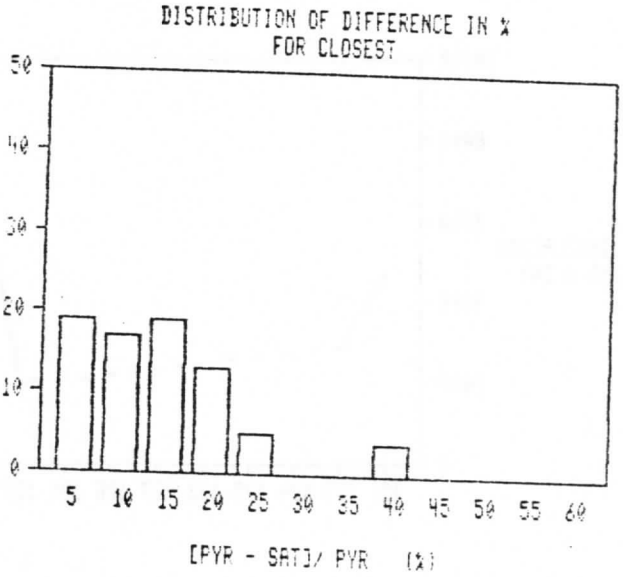
DISTRIBUTION OF DIFFERENCE IN %
FOR CLOSEST
50
40
30
20
10
0
5 10 15 20 25 30 35 40 45 50 55 60
[PYR - SAT]/ PYR (%)

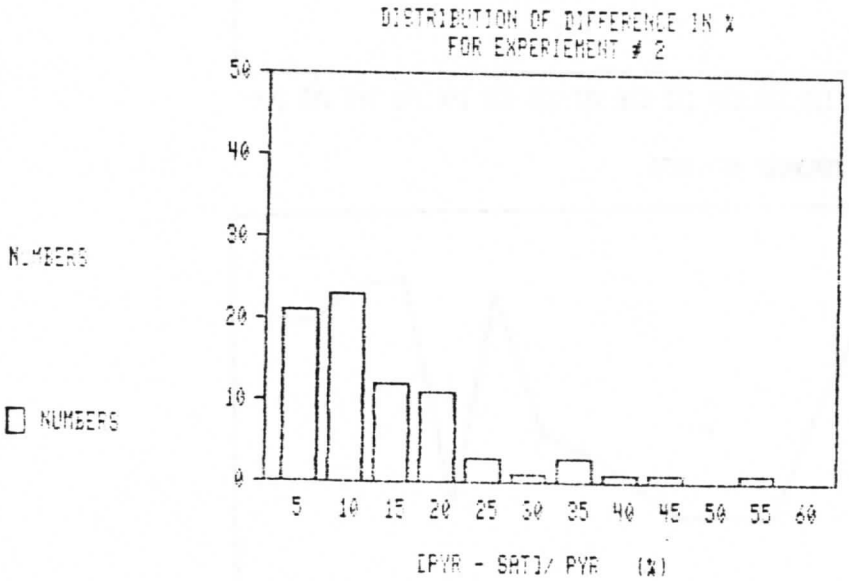
DISTRIBUTION OF DIFFERENCE IN %
FOR EXPERIEMENT # 2
NUMBERS
NUMBERS
50
40
30
20
10
0
5 10 15 20 25 30 35 40 45 50 55 60
[PYR - SAT]/ PYR (%)

Figure 4

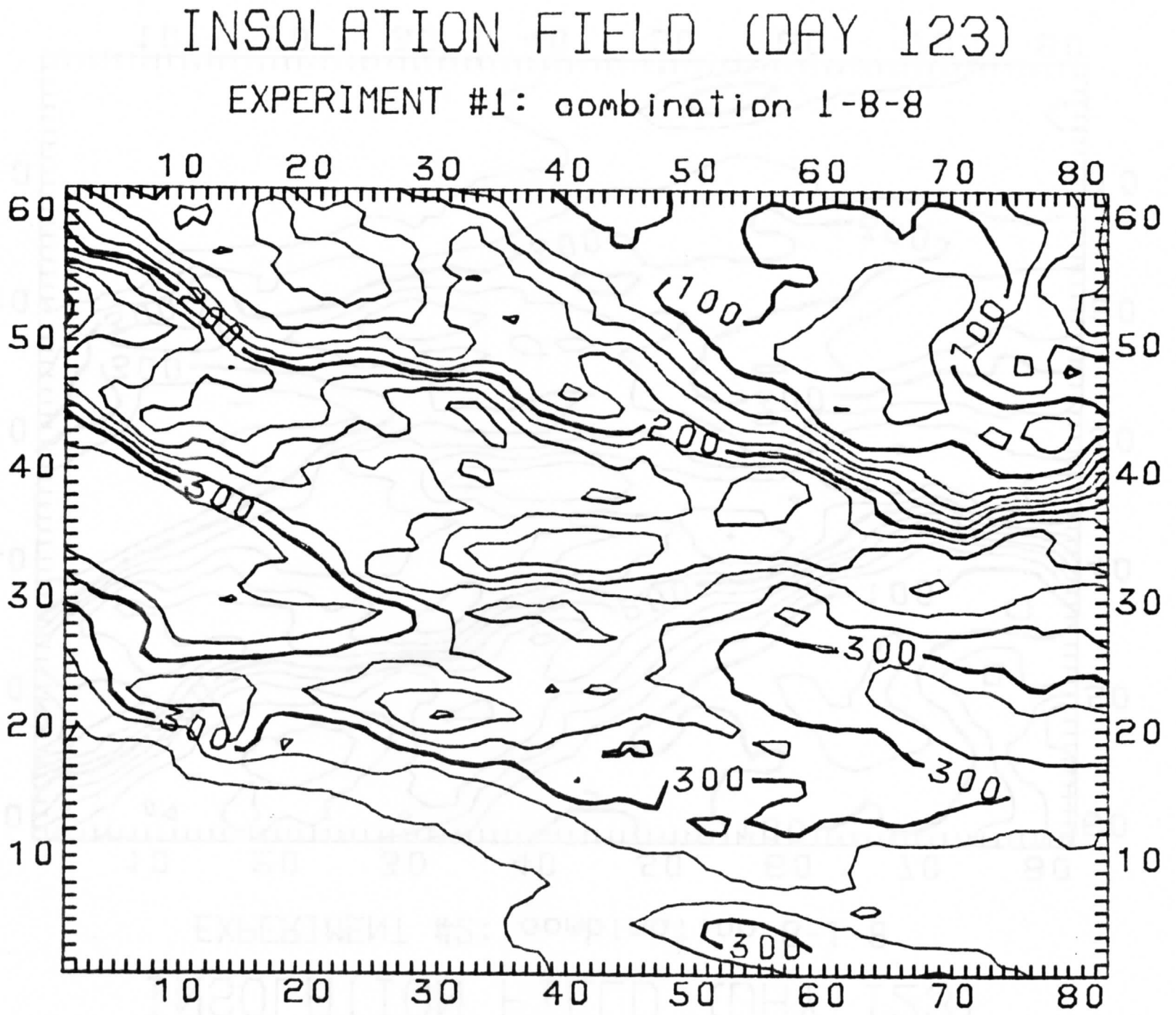
INSOLATION FIELD (DAY 123)
EXPERIMENT #1: combination 1-8-8
10
20
30
40
50
60
70
80
100
200
300

Figure 5

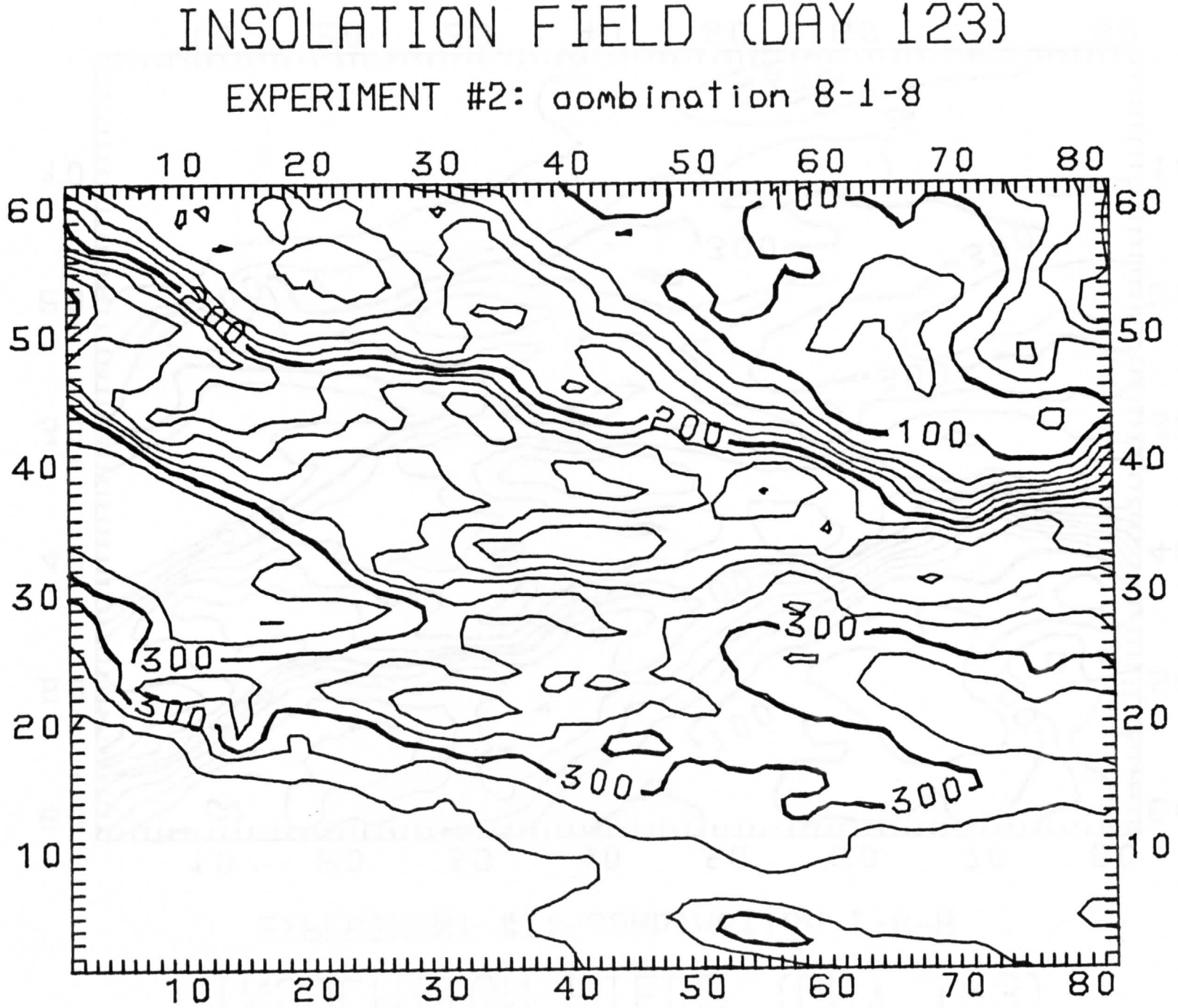
INSOLATION FIELD (DAY 123)
EXPERIMENT #2: combination 8-1-8
10
20
30
40
50
60
70
80
100
200
300

Figure 6

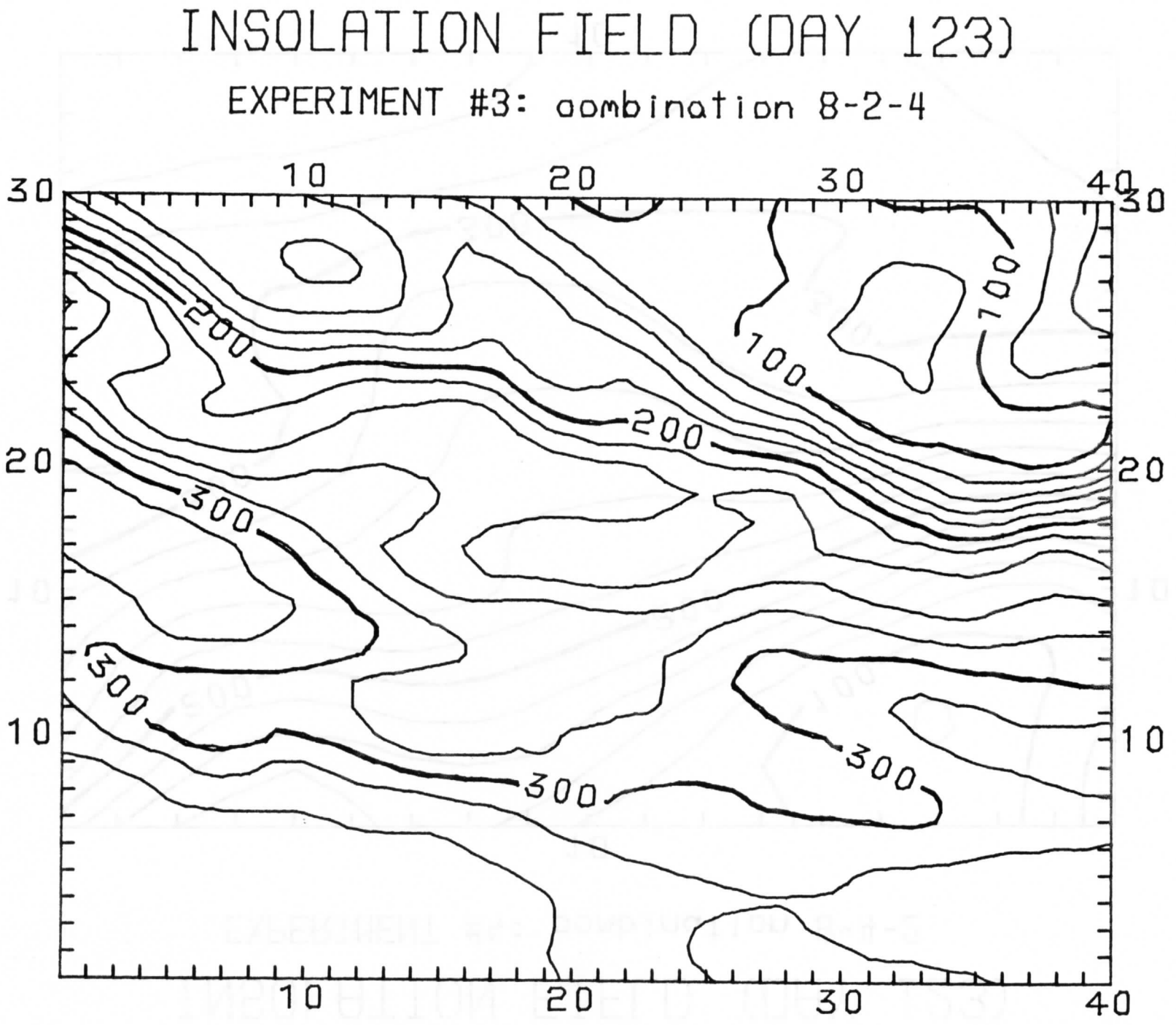
INSOLATION FIELD (DAY 123)
EXPERIMENT #3: combination 8-2-4
10
20
30
40
30
20
10
100
200
300
700

Figure 7

INSOLATION FIELD (DAY 123)

EXPERIMENT #4: combination 8-4-2

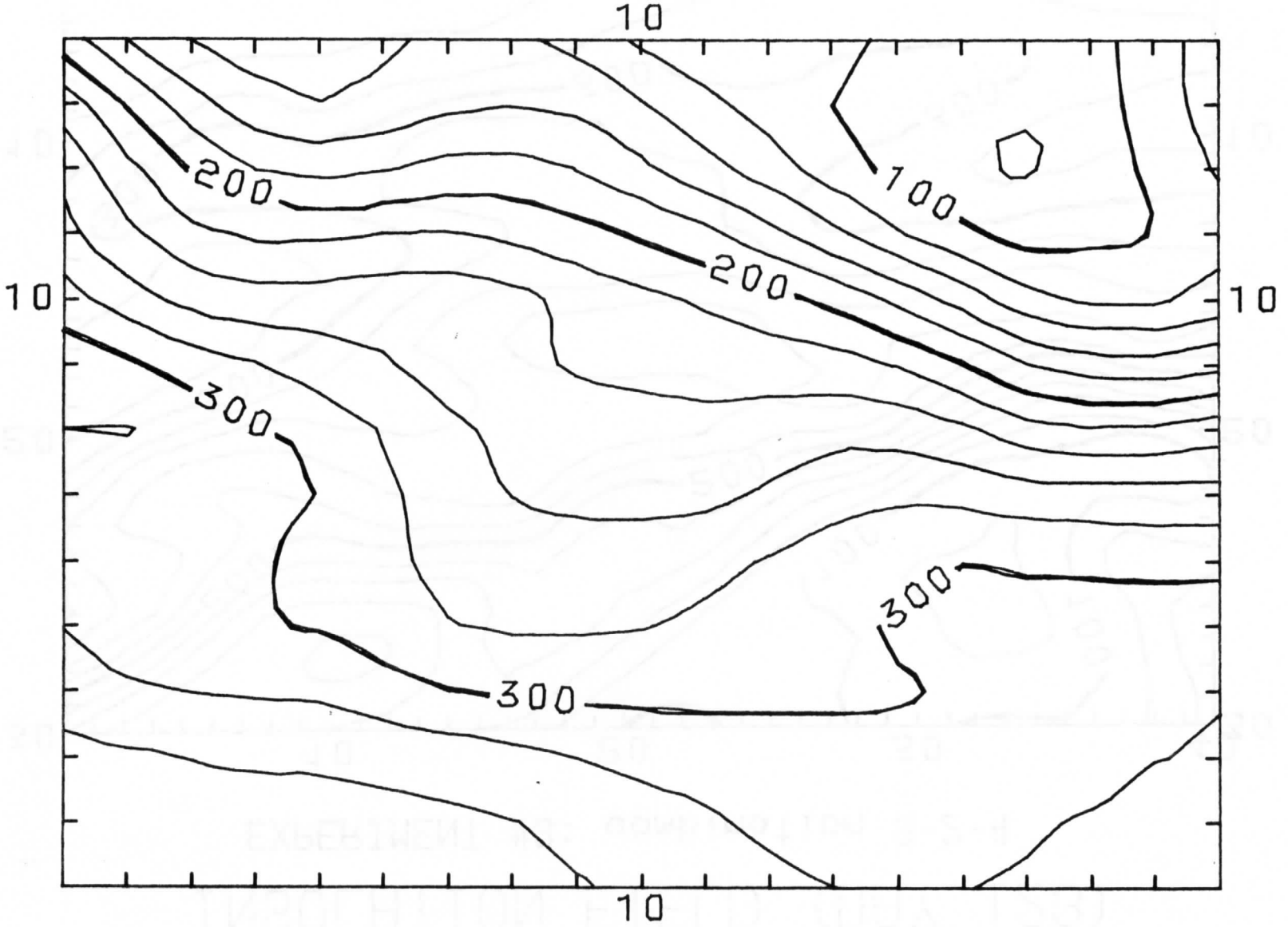

Figure 8

INSOLATION FIELD (DAY 123)

EXPERIMENT #5: oombination 8-8-1

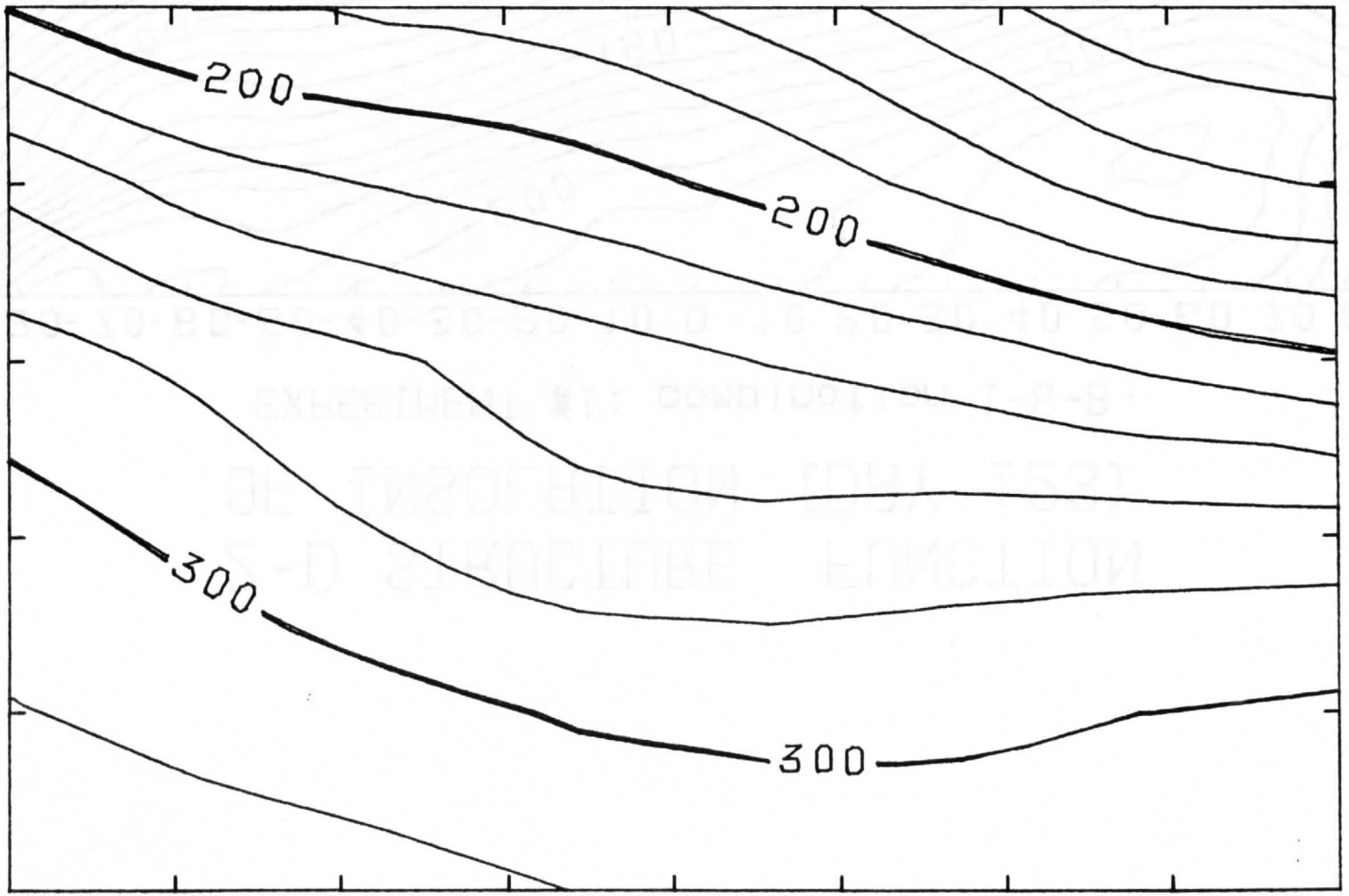

Figure 9

Figure 10

2-D STRUCTURE FUNCTION OF INSOLATION (DAY 123)

EXPERIMENT #1: combination 1-8-8

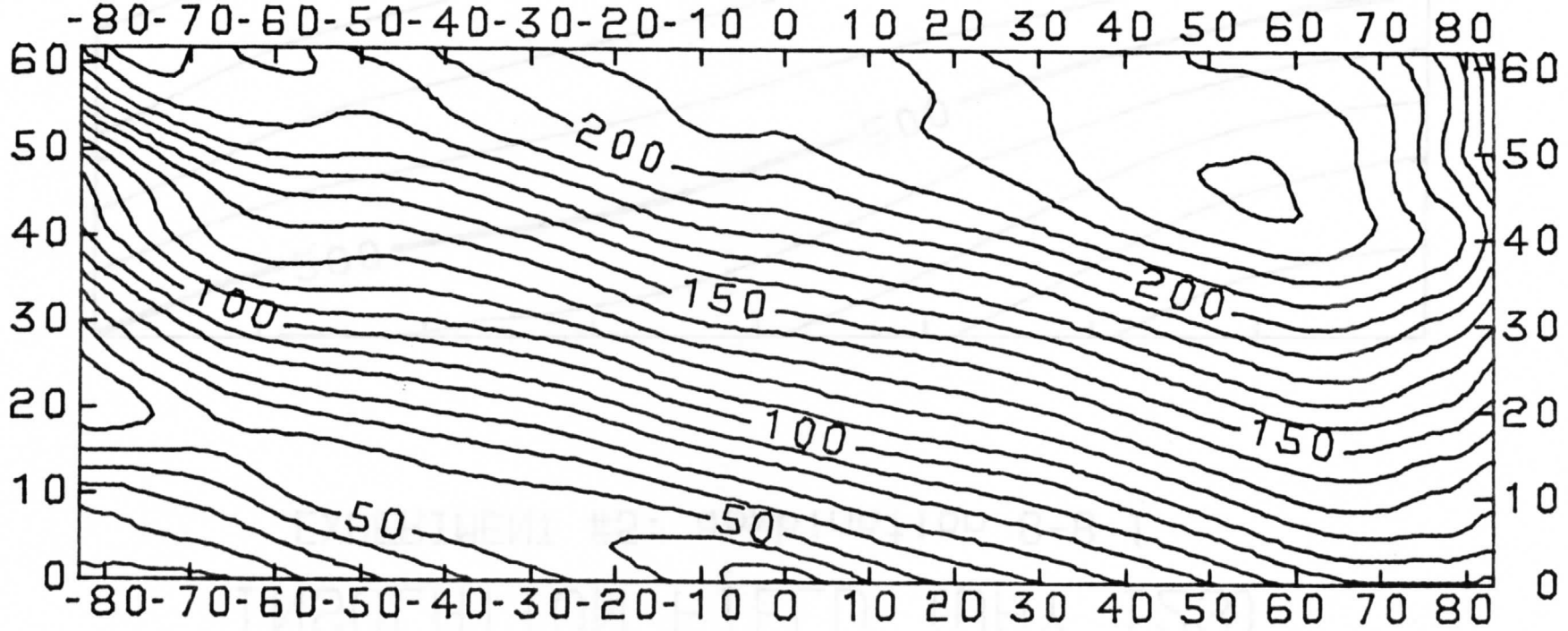

/19/83 3:04 PM

Figure 11

2-D STRUCTURE FUNCTION OF INSOLATION (DAY 123)

EXPERIMENT #2: combination 8-1-8

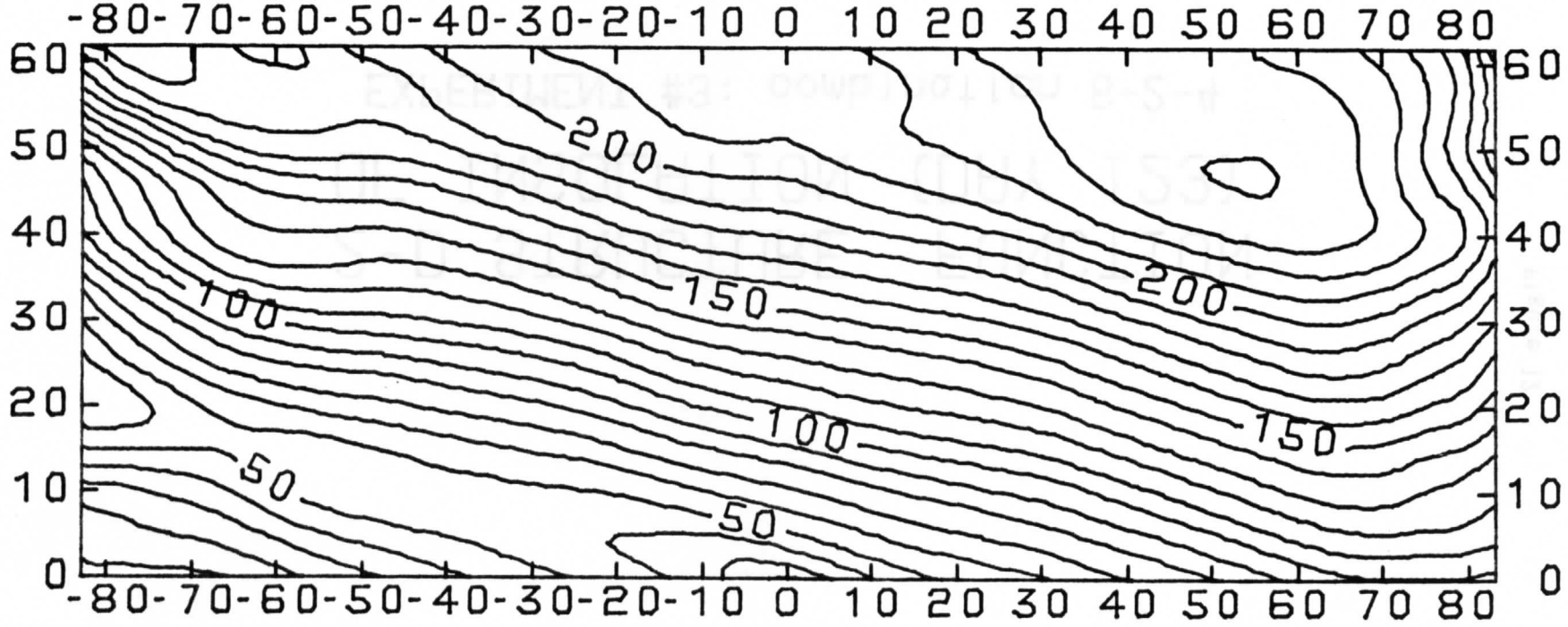

19/83 3:12 PM

2-D STRUCTURE FUNCTION OF INSOLATION (DAY 123)

EXPERIMENT #3: combination 8-2-4

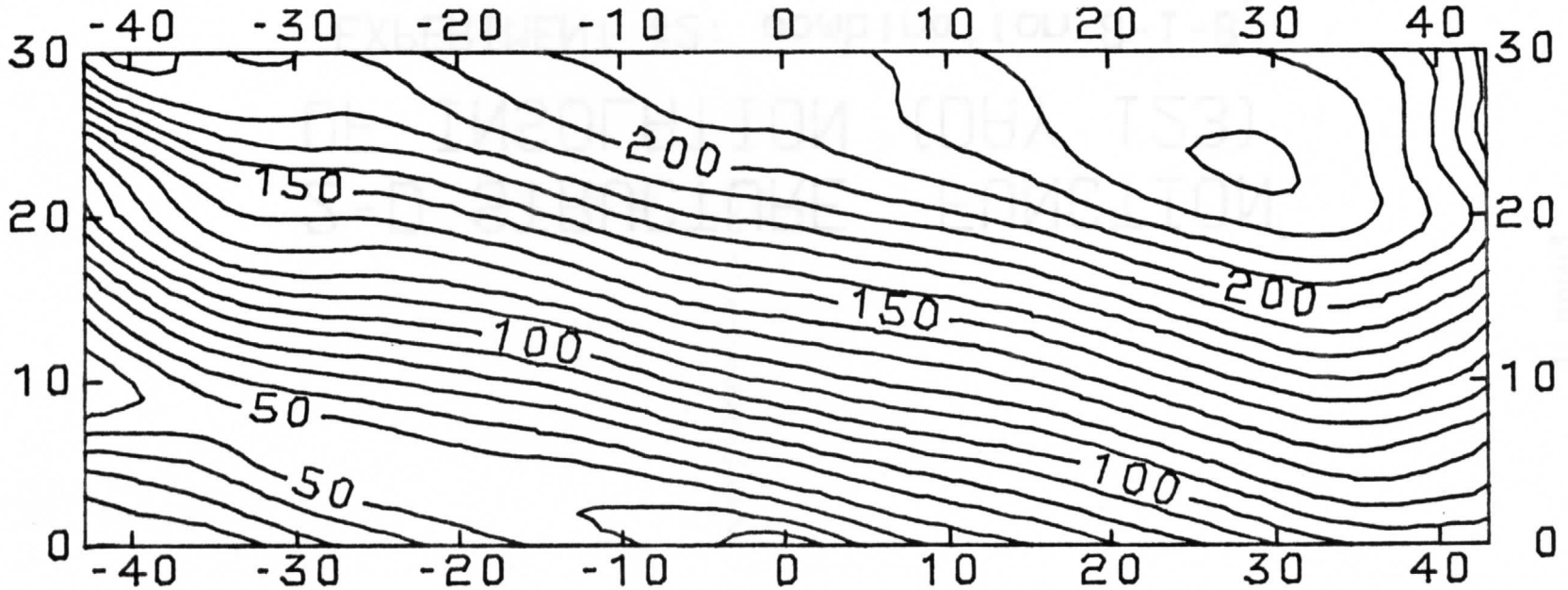

Figure 12

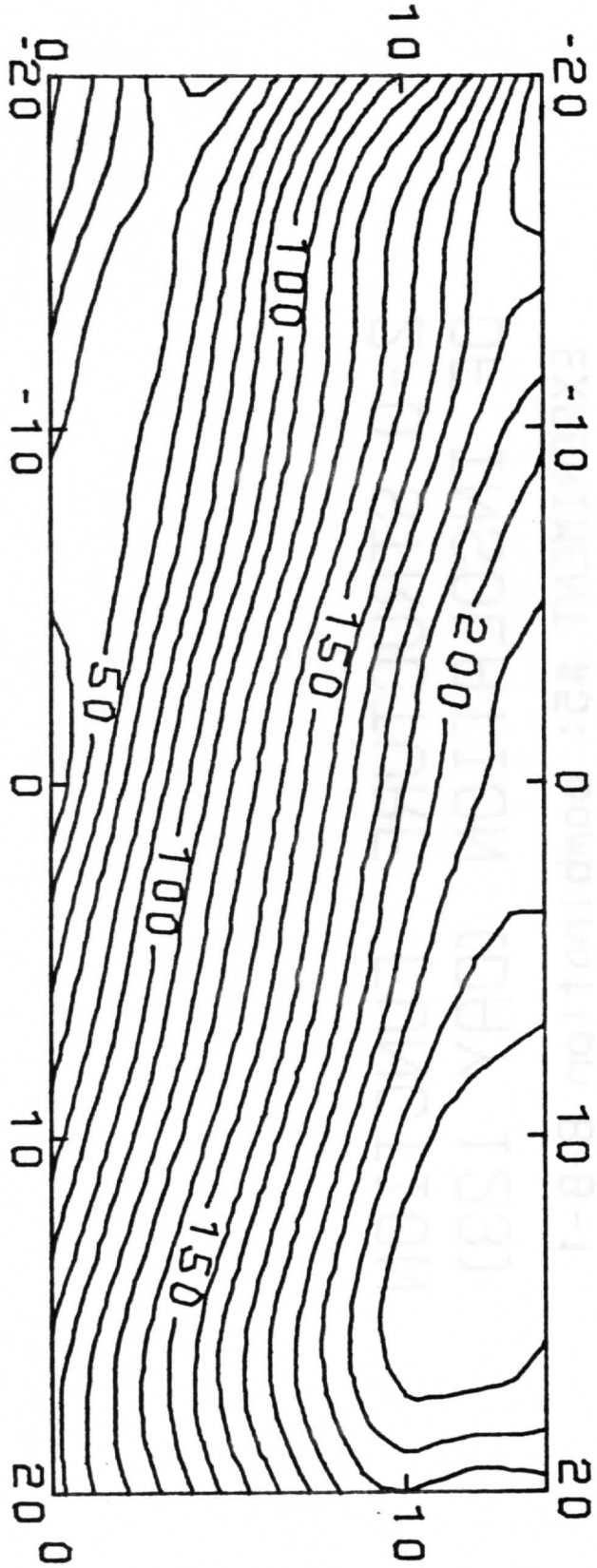
2-D STRUCTURE FUNCTION
OF INSOLATION (DAY 123)
EXPERIMENT #4: combination 8-4-2
-20
-10
0
10
20
100
150
200
50
100
150

Figure 13

19/83 3:42 PM

2-D STRUCTURE FUNCTION OF INSOLATION (DAY 123)

EXPERIMENT #5: combination 8-8-1

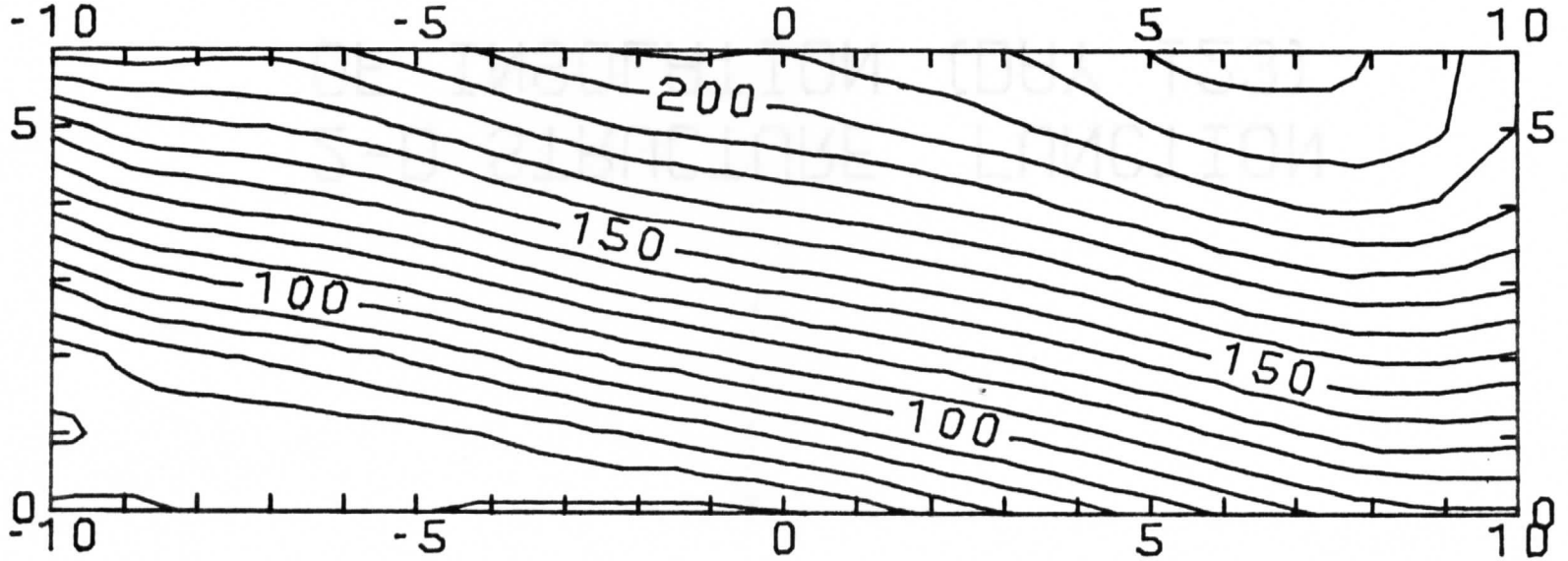

Figure 14

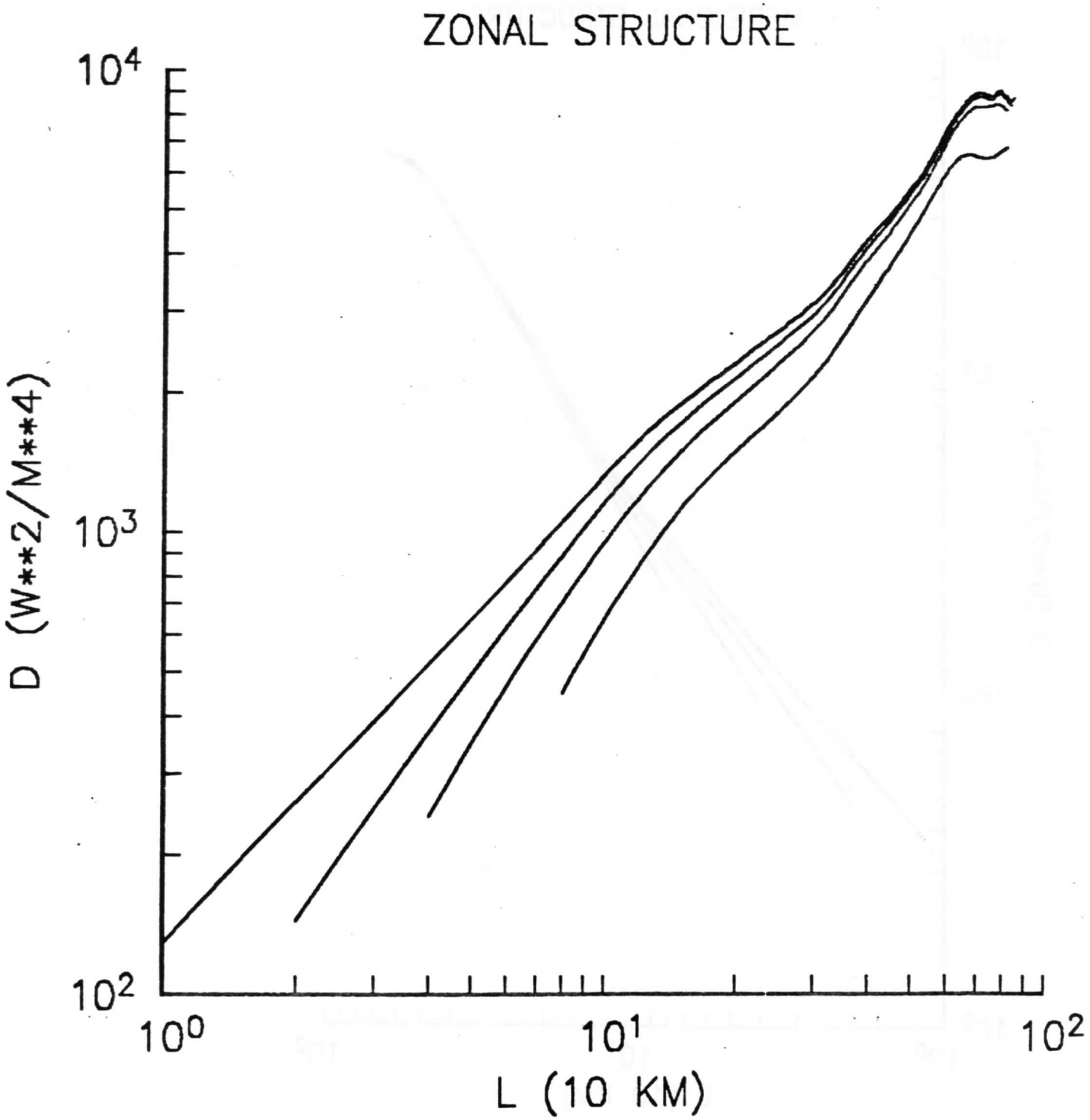

Figure 16

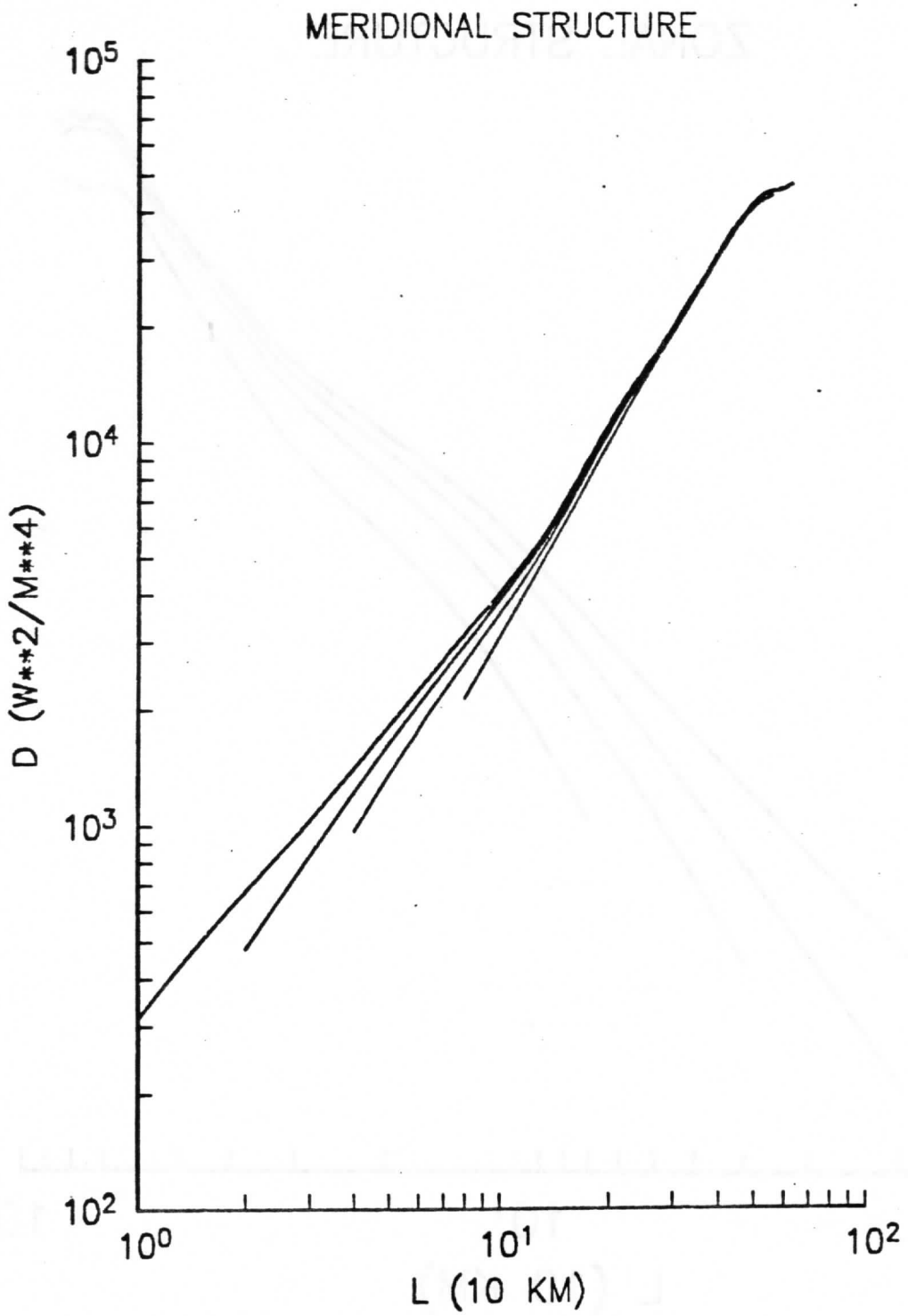

Figure 15